ELECTROCHEMICAL AND OPTICAL INVESTIGATION AND DFT CALCULATION ON TWO TETRAHYDROACRIDINES

Madalina Marina HRUBARU[1,2], Francis Aurelien NGOUNOUE KAMGA[3], Nathanael MURAT[4], Amalia STEFANIU[5], Eleonora-Mihaela UNGUREANU[6*], Elena DIACU[6]

Electrochemical and optical investigations were carried out on 1,2,3,4-tetrahydroacridine-9-carboxamide and 1,2,3,4-tetrahydroacridine-9-carboxylic acid to understand the influence of the two functional groups grafted in position 9 on the behavior of these tetrahydroacridines. Their electrochemical properties were studied by cyclic voltammetry (CV), differential pulse voltammetry (DPV) and rotating disk electrode voltammetry (RDE). CV, DPV and RDE curves were recorded in dimethylformamide (DMF) in presence of tetrabutylammonium perchlorate (0.1 M) for different concentrations of each target, at different scan rates and electrode rotation rates. The UV-Vis spectra were also recorded in DMF, and the calibration curves were obtained. Computed properties and structural descriptors have been predicted using hybrid density functional B3LYP with the 6-311G (d,p) basis set for these two tetrahydroacridines with geometry optimization, focusing on their reactivity comparation. The curves for the two tetrahydroacridines were examined and compared to explain the differences due the different substitution of tetrahydroacridine skeleton which can lead further to the design of their corresponding dimers intended for pharmaceutical purposes.

Keywords: 1,2,3,4-tetrahydroacridine-9-carboxamide, 1,2,3,4-tetrahydroacridine-9-carboxylic acid, cyclic voltammetry, differential pulse voltammetry, rotating disk electrode voltammetry, UV-Vis spectroscopy, DFT calculation.

[1] PhD, "C. D. Nenitzescu" Institute of Organic and Supramolecular Chemistry", Romanian Academy, Bucharest, Romania, e-mail: madalina_marina@yahoo.com

[2] PhD student, Faculty of Chemical Engineering and Biotechnologies (FCEB), National University of Science and Technology POLITEHNICA of Bucharest (NUSTPB), Romania, e-mail: madalina_marina@yahoo.com

[3] PhD Eng., Coordination Chemistry Laboratory, Department of Inorganic Chemistry, Faculty of Science, University of Yaounde, Cameroon, e-mail: fr.kamga@gmail.com

[4] Student, FCEB, NUSTPB, Romania, e-mail: murat_nathanael@yahoo.com

[5] PhD. Eng., National Institute for Chemical and Pharmaceutical Research and Development (ICCF) Bucharest, Romania, e-mail: astefaniu@gmail.com

[6] Prof., Doctoral School Chemical Engineering and Biotechnologies, NUSTPB, Romania, *corresponding author's e-mail: em_ungureanu2000@yahoo.com

1. Introduction

Tetrahydroacridines are a class of organic compounds best known for their large medical potential. They are widely explored in the treatment of different diseases such as Alzheimer's disease (AD) [1], tuberculosis [2], and human cancer [3], due to their ability to inhibit topoisomerase enzymes and block DNA transcription [4, 5]. For example, 9-aminotetrahydroacridine (tacrine) was the first drug approved for the treatment of AD but was later withdrawn due to its hepatotoxicity [6]. Furthermore, the presence of an amide group (-NHCO-) and a polyalkylquinoline skeleton in the structure of tetrahydroacridines or their bioisosteres is a common scaffold found in numerous potential acetylcholinesterase inhibitors [7]. They have been known since 1882 when the first synthesis methods were developed, which involve a cyclocondensation of an *o*-aminocarbonyl component (isatin, ortho-aminobenzaldehyde, ortho-aminoketone) with a carbonyl component bearing a reactive methylene group [8-10].

Tetrahydroacridines are molecules containing an annelated quinoline skeleton with saturated rings. They are a subclass of acridines, which are known to be π-conjugated heteroorganic molecules. Due to their electron donation properties [11] they have found applications in cutting-edge fields such as OLED applications [12].

However, the study of their optoelectrical properties is very scarce compared to their acridine counterparts [13]. This paper continues the tetrahydroacridines studies by comparing the electrochemical behavior of previously studied [14] 1,2,3,4-tetrahydroacridine-9-carboxamide (MM1) with 1,2,3,4-tetrahydroacridine-9-carboxylic acid (MM4) aiming to evaluate the effect of the two functional groups in position 9 on the tetrahydroacridine electrochemical behavior. This study was completed by DFT calculations in order to achieve deep structural insights to assess their reactivity and kinetic stability derived from predicted level energy of frontier molecular orbitals HOMO and LUMO. Satisfactory previous attempts to evaluate molecular properties of interest for electrochemical behavior in terms of redox potentials, provided accurate predictions using hybrid functionals as B3LYP [15, 16]. Our goal is to extend this type of *in silico* approach to the structures subject of the present study.

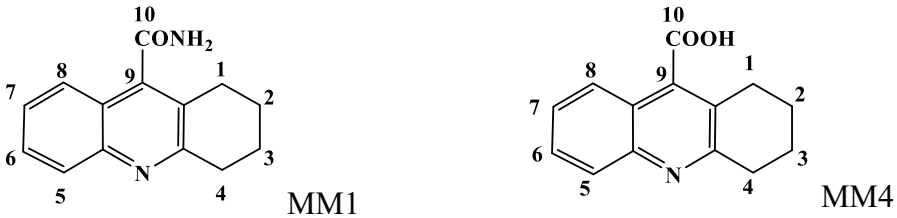

Fig. 1. Investigated ligands with tetrahydroacridine skeleton

2. Experimental

Synthesis of the investigated compounds was performed according to previously described methods [17-20]. The spectral characterization (IR, NMR) confirmed their structure [17c]. High purity acetonitrile (CH_3CN, Sigma Aldrich, 99.999%), dimethylformamide (DMF), and tetrabutylammonium perchlorate (TBAP, Fluka 99.0%) were used (as received). All electrochemical experiments were carried out using a potentiostat Autolab 302N with three-electrodes cells. To perform the electrochemical characterization, a glassy carbon (GC) disk of 3 mm diameter (Metrohm) was used as a working electrode. The counter electrode was platinum wire and the reference electrode was Ag/10 mM $AgNO_3$, 0.1M TBAP/ CH_3CN. Potentials were referred at the end of experiments to the potential of the ferrocene/ferrocenium redox couple (Fc/Fc+) in 0.1 M TBAP/ CH_3CN.

Electrochemical investigations for compounds characterization were performed by cyclic voltammetry (CV), differential pulse voltammetry (DPV) and rotating disk electrode voltammetry (RDE), following similar procedures [21]. The GC working electrode surface was polished before each determination with diamond paste, then wiped with fine paper.

Optical studies on the studied compounds were carried out on the JASCO V-670 spectrophotometer in quartz cuvettes of 1 cm length in dimethylformamide solutions. Aliquots of compound solutions were added to dimethylformamide and a UV–visible spectrum (800–200 nm) was recorded after each addition. A calibration curve was used for each data set to accurately determine compound concentration.

Computational calculation on the B3LYP/6-31G(d,p) optimized geometries of MM1 and MM4 structures was carried out using Spartan14 software (Wavefunction, Inc. Irvine CA, USA) [22] for the lowest energy conformers of each structure, in vacuum conditions, in the ground state using DFT models [22]. The B3LYP theory levels (the Becke three-parameter hybrid exchange functional with the Lee–Yang–Parr correlation functional) [22b] with the 6-311G(d,p) basis set [23] were chosen for the property calculations.

3. Results

3.1. Electrochemical results

The electrochemical behavior of the two tetrahydroacridines MM1 and MM4 was carried out in similar conditions in DMF solutions on glassy carbon (GC) electrode in the potential range between -3.5 V and +2 V. The potential axes were finally referred to the potential of the ferrocene/ferrocenium redox couple (Fc/Fc^+) to compare the compounds.

Current values for the anodic and cathodic processes were examined and attributed to compound's electrooxidation and electroreduction. The curves for

MM1 have been discussed previously [14]. The study of electrochemical processes of MM4 was performed by CV, DPV, and RDE at different concentrations. The peaks were denoted in the order of their apparition in the DPV anodic (a1) and cathodic (c1, c2) scans. In addition, a signal for the solvent reduction appears at -3.2 V (cs) which corresponds to the reduction of the background (Fig. 2). The CV study was also done at different scan rates on various potential ranges.

The DPV and CV curves for MM4 at different concentrations are shown further in Figs. 2a, 3a. Their comparison with MM1 can be seen in Figs. 2b and 3b (for the same concentration of each compound). The values of peak potentials were given in Table 1. The RDE curves for MM4 at different concentrations are shown in Fig. 4a, and the comparison with MM1 in Figs. 4b, 4c and 4d for the same concentration and different rotation rates.

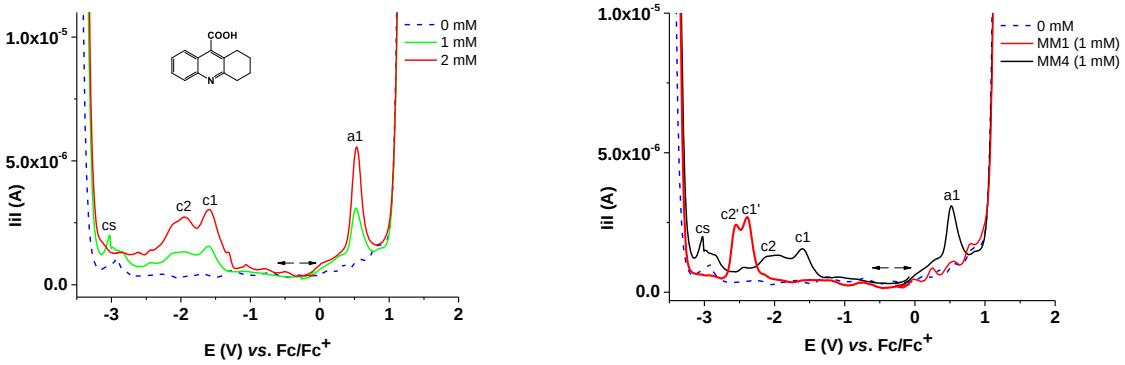

Fig. 2. DPV curves for MM4 at diferent concentrations (a) and comparison between MM1 and MM4 (b) DPV curves at the same concentrations of 1 mM

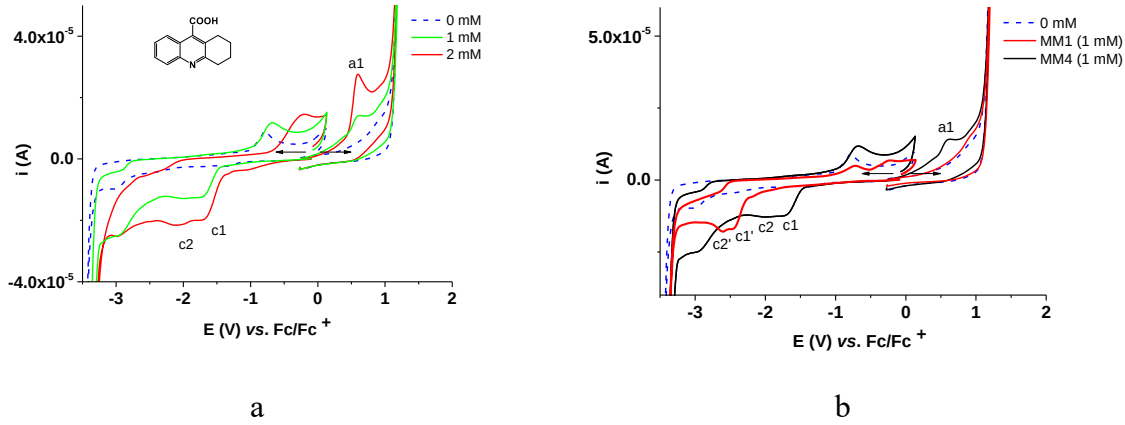

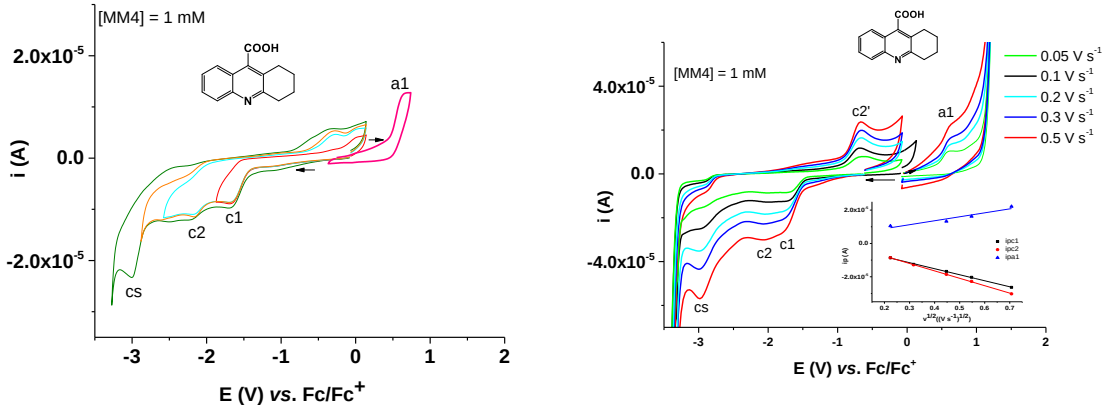

c d

Fig. 3. CV (0.1 V/s) curves for: MM4 at different concentrations (a); comparison between MM1 and MM4 (b) CV curves at the same concentrations of 1 mM; MM4 (1 mM) on different potential domains (c); CV curves for MM4 (1 mM) at different scan rates (d); (d) inset: linear dependences of the peak currents for a1, c1 and c2 processes on the square root on the scan rates

Table 1

Values for the main peak potentials from CV and DPV curves recorded in millimolar solutions of MM1 and MM4 in DMF solvent in presence of 0.1 M TBAP

Peak\ Parameter	E_{CV}(V) MM1	E_{DPV}(V) MM1	E_{CV}(V) MM4	E_{DPV}(V) MM4
a1	-	-	0.598	0.529
c1	-2.460	-2.405	-1.729	-1.599
c2	-2.794	-2.589	-2.111	-1.946
c2’	-	-	-0.661	-

Table 2

Equations of the linear dependences of the main CV peak currents ip (in A) on square root of the scan rate (v in V/s) in MM4 solution (1 mM) in DMF in presence of 0.1 M TBAP

compound	Parameter	ip *vs* $v^{1/2}$	Pearson’s R
MM4	a1	ipa1(0.616 V) = $4.117 \cdot 10^{-6} + 2.376 \cdot 10^{-5} \cdot v^{1/2}$	0.9605
	c1	ipc1(-1.763 V) = $-7.138 \cdot 10^{-7} - 3.611 \cdot 10^{-5} \cdot v^{1/2}$	-0.9994
	c2	ipc2(-2.057 V) = $1.323 \cdot 10^{-6} - 4.446 \cdot 10^{-5} \cdot v^{1/2}$	-0.9999

Table 3

Calculation variants of the diffusion coefficient for MM4 in DMF using the slopes of the fitted lines for the main CV currents peaks for MM4 (1 mM) in 0.1 M TBAP/ DMF

Crt. Nr.	Reference peak	n	E (V)	Slope (A / (V/s)$^{1/2}$)	$10^5 \cdot D_{DMF}$ (cm^2/s)
1	c1	1	-1.763	$3.611 \cdot 10^{-5}$	0.36
2	c1	2	-1.763	$3.611 \cdot 10^{-5}$	0.05
3	c2	1	-2.057	$4.446 \cdot 10^{-5}$	**0.55**
4	c2	2	-2.057	$4.446 \cdot 10^{-5}$	0.07
5	a1	1	0.616	$2.376 \cdot 10^{-5}$	0.16
6	a1	2	0.616	$2.376 \cdot 10^{-5}$	0.02

The absolute value of the peak currents for MM4 increased linearly with the square root of the scan rate (Fig. 3). This indicates these processes are diffusion controlled [14].

The dependence of the cathodic and anodic currents on the square root of the scan rate for MM4 (Table 2) from Fig. 3d inset allowed the estimation of the diffusion coefficient of MM4 in DMF (Table 3), with the help of Randles-Sevcik equation (1) for the CV voltametric peaks, as previously seen in [14].

$$ip = 2.68 \cdot 10^5 \cdot n^{3/2} \cdot A \cdot C \cdot D^{1/2} \cdot v^{1/2} \quad (1)$$

The diffusion coefficient was calculated in DMF (Table 3) using the dependencies of the reduction currents for peak c2 and considering the same mechanism [14] for the electrochemical reduction. The value of the diffusion coefficient in DMF for MM4 ($D_{MM4, DMF}$) is $0.55 \cdot 10^{-5}$ $cm^2 \cdot s^{-1}$.

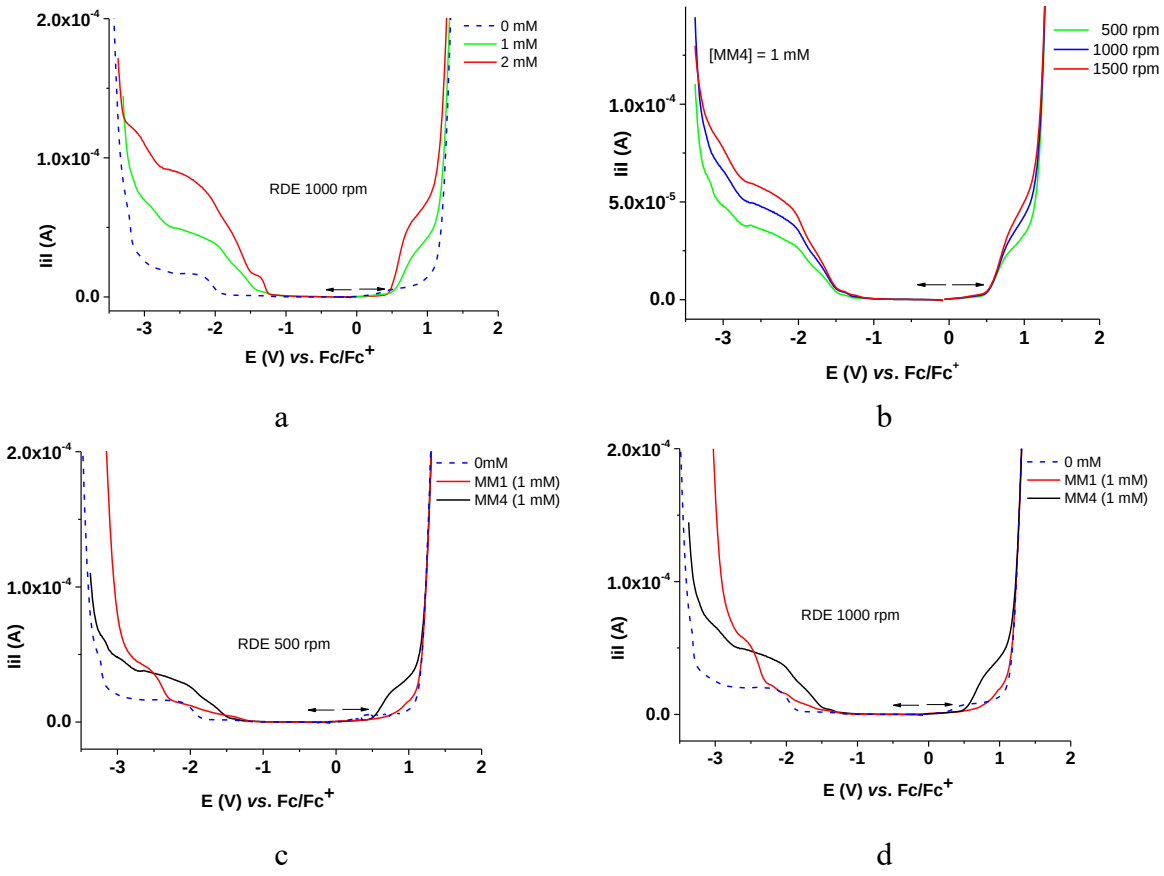

Fig. 4. RDE curves for MM4 at diferent concentrations (a) and rotation rates (b), and comparison between MM1 and MM4 at two rotation rates (c, d) for the same concentration of MM4 (1 mM)

The results of electrochemical studies on MM4 enlarge the known properties of tetrahydroacridines and provide the basis for understanding the electrochemical properties of other important derivatives.

3.2. UV-Vis spectra

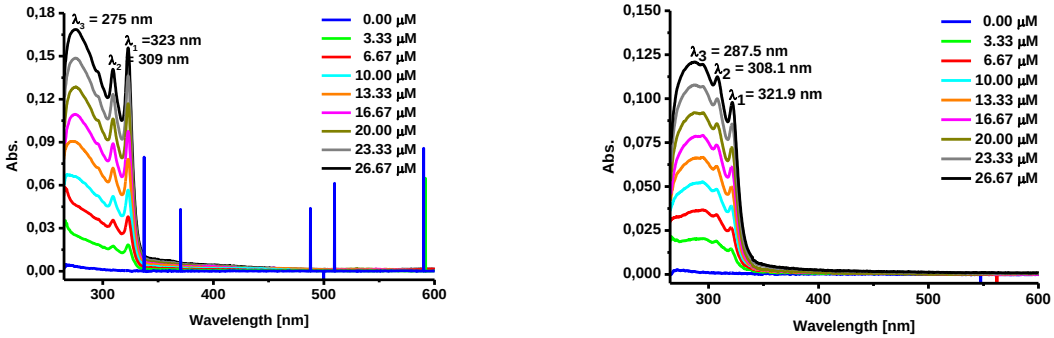

a b

Fig. 5. UV-Vis spectra in DMF for MM1 (a) and MM4 (b) at different concentrations

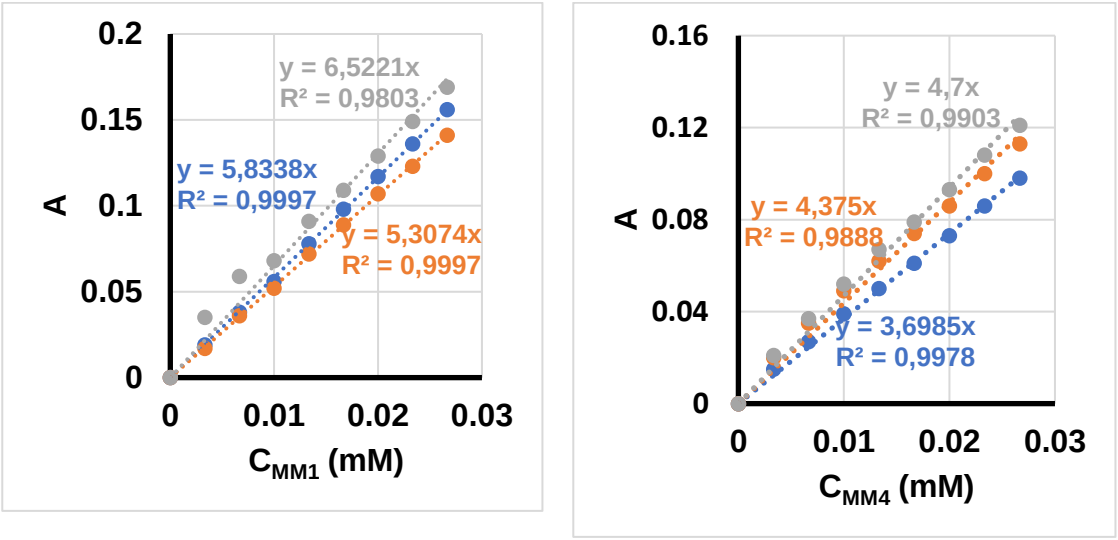

a b

Fig. 6. Linear dependencies of absorbance on concentration for MM1 (a) and MM4 (b) in DMF at the main peak wavelengths

The UV-Vis spectra of MM1 and MM4 showed three main absorption bands (Fig. 5). The evolution of the absorbance at these wavelengths with concentration of tetrahydroacridine is linear with higher slopes for MM1 than for MM4 (Fig. 6).

From the absorbance slopes as functions of concentration, their extinction coefficients were calculated (Table 4).

Table 4

Main peak wavelengths and equations for the linear dependences of absorbance on concentration for MM1 and MM4 solutions in DMF

Compound	λ_{max} [nm]	A *vs.* C (mM) equation	Pearson's R	ε [M^{-1}•cm^{-1}]
MM1	323.00 (= $\lambda_{1, MM1}$)	A = 5.875•C - 0.001	0.9997	5833.8
	309.00 (= $\lambda_{2, MM1}$)	A = 5.305•C + 0.000	0.9997	5307.4
	275.00 (= $\lambda_{3, MM1}$)	A = 5.995•C + 0.010	0.9803	6522.1
MM4	321.90 (= $\lambda_{1, MM4}$)	A = 3.595•C + 0.002	0.9978	3698.5
	308.10 (= $\lambda_{2, MM4}$)	A = 4.095•C + 0.005	0.9888	4375.0
	287.50 (= $\lambda_{3, MM4}$)	A = 4.420•C + 0.005	0.9903	4700.0

3.3. Results of DFT calculation

Linear relationships between calculated HOMO and LUMO energies and experimental oxidation and reduction potentials were found for both compounds. The calculations followed similar procedures [24]. The results of the property calculations based on electron density are presented in Table 5 and Table 6. The electrostatic potential maps for MM1 and MM4 are shown in Fig. 8. The color indicates the value of the electrostatic potential, according to the given lateral scale. Red areas suggest negative potential, the color tending towards blue denotes regions of positive potential. The potential increases in the order: red < orange < yellow < green < blue.

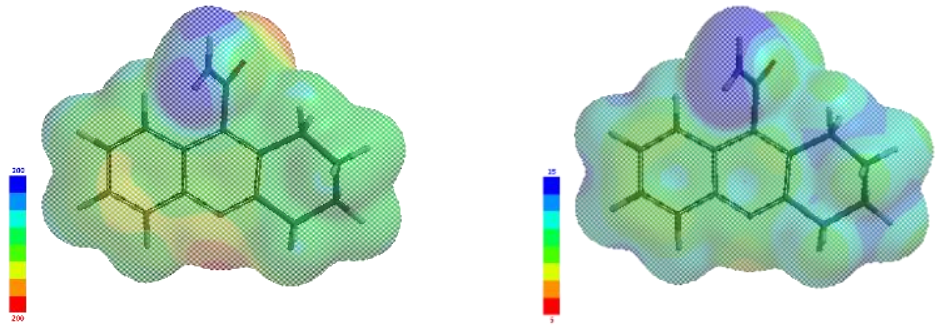

a b

Fig. 7. Electrostatic potential maps predicted for MM1 (a) and MM4 (b)

The red regions have a different intensity on the two compounds, being more pronounced on MM1 and almost absent on MM4, in accordance with the minimum values found for the electrostatic potential of -192.21 kJ·mol^{-1} for MM1, and -

178.70 kJ·mol^{-1} for MM4, as shown in Table 5 (line 16). More negative potential is consequently illustrated by blue regions on the electrostatic potential map of MM1.

Table 5

Molecular properties (lines 1 to 7) and QSAR (lines 8 to 16) predicted for MM1 and MM4

No.	Parameter\Compound	MM1 $C_{14}H_{14}N_2O$	MM4 $C_{14}H_{13}NO_2$
1	Molar mass (g · mol^{-1})	226.279	227.263
2	Energy (a.u.)	-726.85	-746.71
3	Energy (aq) (a.u.)	-726.86	-746.73
4	Solvation energy (kJ · mol^{-1})	-39.65	-36.39
5	Dipole moment (Debye)	3.26	2.76
6	E_{HOMO} (eV)	-6.38	-6.70
7	E_{LUMO} (eV)	-1.72	-2.12
8	Area (Å^2)	246.16	239.43
9	Volume (Å^3)	234.60	231.15
10	PSA (Å^2)	45.752	39.025
11	Ovality index	1.34	1.31
12	Polarizability (10^{-30} · m^3)	59.30	59.04
13	LogP	2.29	2.94
14	HBD Count	1	1
15	HBA Count	3	2
16	MinElPot (kJ · mol^{-1})	-192.21	-178.70

Table 6

Values of quantum chemical reactivity parameters (in eV) of MM1 and MM4

No.	Parameter\Compound		MM1	MM4
1	I = ionization potential	$I = - E_{HOMO}$	6.38	6.70
2	A = electron affinity	$A = - E_{LUMO}$	1.72	2.12
3	ΔE = energy gap	$\Delta E = I - A$	4.66	4.58
4	χ = electronegativity	$\chi = (I + A)/2$	4.05	4.41
5	η = overall hardness	$\eta = (I - A)/2$	2.33	2.29
6	σ = overall softness	$\sigma = 1 / \eta$	0.43	0.44

The density distribution of the frontier molecular orbitals obtained by calculation for the studied structures is represented by Fig. 8, as well as the energy diagram and the gaps (ΔE) between HOMO and LUMO.

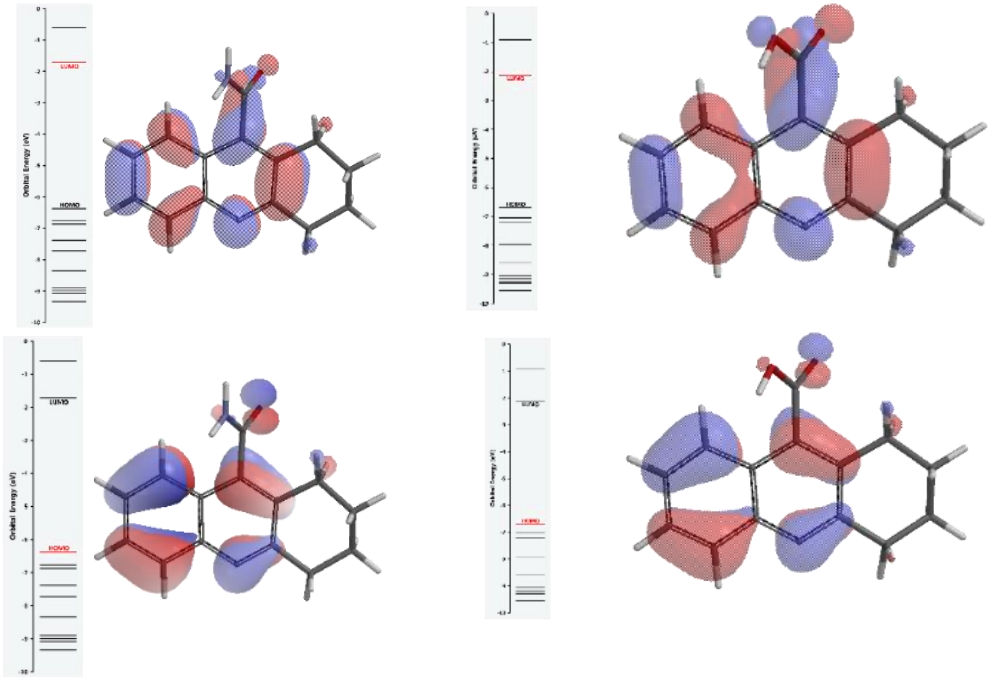

a b

Fig. 8. HOMO (bottom)-LUMO (up) energy diagrams for MM1 (a) and MM4 (b)

From the E_{HOMO} and E_{LUMO} levels of energy provided in Table 5, other associated quantum descriptors are calculated. Table 6 gives the relationships and the resulted values for: the energy gap (ΔE), the ionization potential (I), the electron affinity (A), the electronegativity (χ), the overall hardness (η), the overall softness (σ) [25,26], and the overall electrophilicity index (ω) [27] using the B3LYP/6-311G (d,p) density functional model. I and A were predicted by through the use of the equations proposed by Koopmans [28, 29]. Other descriptors such as the softness (σ) and hardness (η) are based upon Pearson's principle of hard and soft acids and bases (HSAB) [30], and the maximum hardness principle (MHP) [31] giving indications about electronic reactivity and response to electronic disturbances, respectively. The overall electrophilicity index (ω), as stated by Parr R.G and co-workers [27], describes the reactivity of chemical entities in different solvents or biological environments.

4. Discussion

4.1. Electrochemical experiments for MM4 vs. MM1

DPV experiments. The DPV curves for MM4 at different concentrations shown in Fig. 2a, as well as their comparison with MM1 curves in Fig. 2b for the same concentration of compounds show the DPV oxidation and reduction processes

occur easier for MM4 than for MM1 (the anodic and cathodic peaks potential values given in Table 1 are the proof). The first cathodic peaks for each compound were denoted c1 and c1', respectively, in Fig. 2b. They were attributed to the same process of double C=N bond reduction, as previously discussed [14]. This is a result which agrees with the DFT calculations for the two compounds from which the carboxylic acid MM4 shows an increased reactivity compared to the MM1. MM4 has an intense anodic oxidation peak a1, unlike MM1 which does not present any peak in the accessible potential range in DMF, a1 could be due to the oxidation of carboxylic (-COOH) group.

CV experiments. The CV curves for MM4 at different concentrations shown in Fig. 3a, and the comparison between MM1 and MM4 in CV given in Fig. 3b for the concentrations of 1 mM for each compound indicated the currents are increasing with concentration, allowing selecting the peaks due to the processes of each compound. This increase for the anodic and cathodic peaks indicates these peaks are specific for the compound. The differences between the obtained curves for MM1 and MM4 indicate the presence of different functional groups on the tetrahydroacridine ring determines significant changes in terms of position and intensity of the signals recorded, both in the domains of anodic and cathodic potentials. Two cathodic peaks were detected in the case of MM1 and MM4. A broad anodic peak was detected only for MM4. The current intensity values of CV oxidation and reduction currents are of the same order of magnitude. The reduction potentials are connected to the quasi-reversible reduction of the C=N double bond with the formation of a single bond, as resulted from the CV scans on different cathodic domains. The CV curves for MM4 on different potential domains (Fig. 3c) allowed the estimation of each electrochemical process reversibility (both c1 and c2 are quasi-reversible). The absence of an oxidation peak in case of MM1 in comparison with MM4 means MM1 oxidizes more difficult than MM4 (at a more positive potential). The effect of the scan rate on the peaks current shapes of MM4 indicated linear relationships between the peak current (ip) and the square root of the scan rate in the potential domains of a1, c1 and c2 peaks. The equations of these linear dependencies of the main CV peaks currents given in Table 2 allowed the calculation of diffusion coefficients for MM4 from their slope. The obtained value $D_{MM4} = 0.55 \cdot 10^{-5}$ $cm^2 \cdot s^{-1}$ indicates a lower electrochemical kinetics in reduction for MM4 than for MM1 ($D_{MM1} = 0.82 \cdot 10^{-5}$ $cm^2 \cdot s^{-1}$ [14]). In oxidation the behavior is reversed: MM4 has a higher rate of electrochemical oxidation than MM1. From thermodynamic point of view MM4 is also more reactive than MM1, as its oxidation potential is lower.

RDE experiments. RDE curves for MM1 shown in Fig. 4 indicate a regular behaviour for anodic and cathodic processes, with limiting currents increasing with concentration (Fig. 4a). However, the influence of the rotation rate for cathodic and

anodic processes (Fig. 4b) is different, the anodic currents being less influenced than the cathodic ones. The comparison between RDE curves for MM1 and MM4 made on the same concentration (Fig. 4c, 4d) indicates controlled diffusion processes situated at different potentials at all rotation rates, which reflects differences between the two investigated compounds, the results being in accord with the DPV and CV differences.

Comparison between electrochemical methods. The DPV, CV and RDE curves for MM1 and MM4 are correlated in Fig. 9. The DPV curves are presented in parallel with those obtained by CV and RDE to compare their processes occurring at potentials given in Table 1. The differences between the two investigated compounds are better stressed by RDE method (Fig. 9c, 9d), the results being in accord with the DPV and CV methods (Fig. 9a, 9b). The comparison between the methods applied to evidence the behaviour of MM1 and MM4 (Fig. 9) is favorable for RDE with shows important variation of the currents with concentration in case of MM4 (Fig. 9c, 9d). This is due to the supply of substance brought by convection to the surface of the electrode due to its rotation, which determines an increase in the rate of electrochemical processes that take place at a certain potential leading to a better differentiation of the investigated substrates, compared to the methods that are based only on diffusion (DPV, CV).

4.2. UV-Vis spectra for MM1 and MM4

Both MM1 and MM4 present three main absorption bands in UV-Vis at closed wavelengths. Their absorbances are linear with higher slopes for MM1 than for MM4. The extinction coefficient of MM1 is bigger than that for MM4 at all wavelengths, showing a more extensive conjugation via -$CONH_2$ than through -COOH.

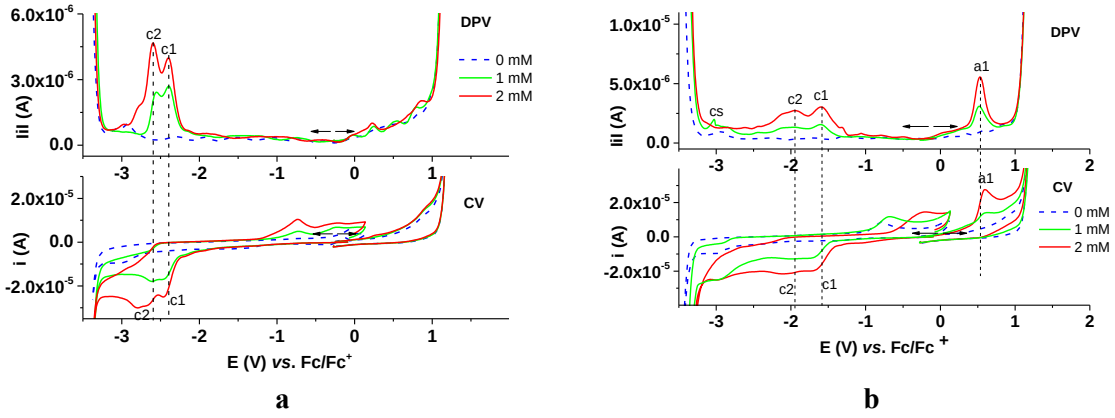

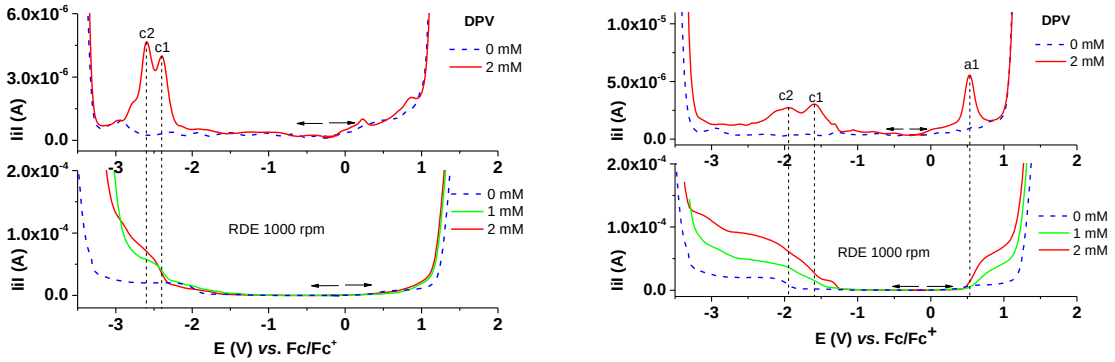

Fig. 9. DPV(up) and CV (down) curves for MM1 (a) and MM4 (b) at different concentrations; DPV (up) and RDE (down) for MM1 (c) and MM4 (d) at different concentrations

4.3. DFT calculations for MM1 and MM4

Considering the value obtained for the energy gap between the frontier molecular orbitals, the compound MM1 seems more stable and less reactive than MM4, for which the electronic jump is easier to achieve. The similarity of the chosen structures is also visible regarding the distribution of molecular orbitals shown in Fig. 8, where the slight difference is made by the distribution of LUMO orbitals on the benzene ring, showing a more extended delocalization of the LUMO orbital due to the carboxyl function.

5. Conclusion

The electrochemical and optical investigations carried out on two tetrahydroacridines functionalized at the position 9 of the tetrahydroacridine skeleton with carboxyl and carboxamide groups allowed to put in evidence the effect of these functional groups on the properties of selected compounds. The electrochemical study performed by three methods leads to similar conclusions concerning the reactivity of 1,2,3,4-tetrahydroacridine-9-carboxylic acid and 1,2,3,4-tetrahydroacridine-9-carboxamide. The curves recorded by RDE highlighted the differences between them compared with those recorded by CV and DPV. However, the DPV curves let to get the potentials where oxidation and reduction processes occur, being in a good agreement with the potentials found by CV. Each method proved to be compulsory for the electrochemical characterization of these tetrahydroacridines.

The UV-Vis study of these compounds allowed the calculation of their extinction coefficients. Their computations revealed that the ionization potential and electronic affinity of the acid are higher than those for carboxamide derivative, together with the value of the HOMO-LUMO gap (ΔE). The carboxamide

derivative reveals lower electrostatic potential on heteroatoms regions, but overall, slight difference in reactivity, compared to acid derivative.

Acknowledgement:

The authors acknowledge National University of Science and Technology Politehnica of Bucharest for materials support; the authors are thankful to Agence Universitaire de la Francophonie for the support through the grant Petrache Poenaru.

R E F E R E N C E S

[1]. *B. Dogga, Eeda, K. Reddy, C.S. Sharanya, J. Abhithaj, K.G. Arun, C.S. Ananda Kumar, K.S. Rangappa,* "Design, synthesis and SAR studies of novel tacrine derivatives as potent cholinesterase inhibitors", in European Journal of Medicinal Chemistry Reports., **vol. 6**, 2022, pp. 100094, https://doi.org/10.1016/j.ejmcr.2022.100094

[2]. *R.P. Tripathi, S.S. Verma, Jyoti Pandey, K.C. Agarwal, Vinita Chaturvedi, Y.K. Manju, A.K. Srivastva, A. Gaikwad, S. Sinha*, "Search of antitubercular activities in tetrahydroacridines: Synthesis and biological evaluation", in Bioorg. Med. Chem. Lett., **vol. 16**, no. 19, 2006, pp. 5144-5147, https://doi.org/10.1016/j.bmcl.2006.07.025

[3]. *J. Janockova, J. Korabecny, J. Plsikova, K.B.E. Konkolova, D. Kucerova,J. Vargova,J. Koval, R. Jendzelovsky,P. Fedorocko, J. Kasparkova, V. Brabec, J. Rosocha, O.Soukup, Slavka Hamulakova, K. Kuca, M. Kozurkova,* "In vitro investigating of anticancer activity of new 7-MEOTA-tacrine heterodimers", in J Enzyme Inhib Med Chem., **vol. 34,** no. 1, 2019, pp. 877–897 https://doi: 10.1080/14756366.2019.1593159

[4]. (a) *M.C. Pirrung, J.H. Chau, J. Chen,* "Discovery of a novel tetrahydroacridine acetylcholinesterase inhibitor through an indexed combinatorial library", Chen J. Chem Biol., **vol. 2**, 1995, pp. 621–626. (b) *P. Olszewska, E. Mikiciuk-Olasik, K. Błaszczak-Świątkiewicz, J. Szymański, P. Szymański*, "Novel tetrahydroacridine derivatives inhibit human lung adenocarcinoma cell growth by inducing G1 phase cell cycle arrest and apoptosis", Biomed. pharmacother., **vol. 68**, 2014, pp. 959-967 https://doi.org/10.1016/j.biopha.2014.10.018

[5]. (a) *R.G. Gouveia, A.G. Ribeiro, M. Â. S.P. Segundo, J. F. de Oliveira, M. do C. A. de Lima, T. R. C. de L. Souza, S. M. V. de Almeida, R. O. de Moura*, "Synthesis, DNA and protein interactions and human topoisomerase inhibition of novel Spiroacridine derivatives", in Bioorg. Med. Chem., **vol. 26**, 2018, pp. 5911-5921. (b) *C. Martins, M. C. Carreiras, R. León, C. de los Ríos, M. Bartolini, V. Andrisano, I. Iriepa, I. Moraleda, E. Gálvez, M. García, E. Javier, S. Abdelouhaid, C. Mourad, and M-C. José*, "Synthesis and biological assessment of diversely substituted furo[2,3-b]quinolin-4-amine and pyrrolo[2,3-b]quinolin-4-amine derivatives, as novel tacrine analogues", in Eur. J. Med. Chem., **vol. 46**, 2011, pp. 6119–6130

[6]. *N. Qizilbash, A. Whitehead, J. Higgins, G. Wilcock, L. Schneider, M. Farlow*, "Cholinesterase inhibition for Alzheimer disease: a meta-analysis of the tacrine trials. Dementia Trialists' Collaboration", in JAMA, **vol. 280**, no. 20, 1998, pp. 1777-1782, https://doi: 10.1001/jama.280.20.1777

[7]. *M. Kozurkova, S. Hamulakova, Z. Gazova, H. Paulikova, P. Kristian*, "Neuroactive Multifunctional Tacrine Congeners with Cholinesterase, Anti-Amyloid Aggregation and Neuroprotective Properties", in "Pharmaceuticals", **vol. 4**, 2011, pp. 382–418 https://doi.org/10.3390/ph4020382

[8]. *P. Frielander*, "Ueber o-Amidobenzaldehyd", in Ber. Deutsch. Chem. Ges., **vol. 15**, 1882, pp. 2572, https://doi.org/10.1002/cber.188201502219

[9]. *S. V. Niementowski*, "Synthesen der Chinolinderivate". Chemische Berichte. **vol. 27**, no. 2, 1894, pp. 1394–1403 https://doi:10.1002/cber.18940270242
[10]. *W.Pfitzinger*, Chinolinderivate aus Isatinsaure", in J.Prakt. Chem., **vol. 33**, no, 2, 1886, pp.100
[11]. (a*) X. Gong, C. H. Lu, W. K. Lee, P. Li, Y. H. Huang, Z. Chen, L. Zhan, C. C. Wu, S. Gong, C. Yang*, "High-efficiency red thermally activated delayed fluorescence emitters based on benzothiophene-fused spiro-acridine donor", Chem. Eng. J., **vol. 405**, 2021, pp. 126663. https://doi.org/10.1016/j.cej.2020.126663; (b) *T. Chen, C.-H. Lu, Z. Chen, X. Gong, C.-C. Wu C. Yang*, "Modulating the Electron-Donating Ability of Acridine Donor Units for Orange–Red Thermally Activated Delayed Fluorescence Emitters", Chem. Eur. J., **vol. 27**, 2021, pp. 3151-3158 https://doi.org/10.1002/chem.202004719
[12]. (a) W. *Zeng, H. Y. Lai, W. K. Lee, M. Jiao, Y. J. Shiu, C. Zhong, S. Gong, T. Zhou, G. Xie, M. Sarma, W. Ken-Tsung, W. Chung-Chih, and Y. Chuluo*, "Achieving Nearly 30% External Quantum Efficiency for Orange–Red Organic Light Emitting Diodes by Employing Thermally Activated Delayed Fluorescence Emitters Composed of 1,8-Naphthalimide-Acridine Hybrids", in Adv. Mater., **vol. 30**, 2018, pp. 1704961. (b) *N. Tka, M. A. H. Ayed, M. Braiek, M. Jabli, P. Langer*, "Synthesis and investigation on optical and electrochemical properties of 2,4-diaryl-9-chloro-5,6,7,8-tetrahydroacridines", in Beilstein. J. Org. Chem., 2021, **vol. 17**, 2450–2461 https://doi: 10.3762/bjoc.17.162
[13]. (a) *J. Zhang, J. R. Lakowicz*, "Enhanced Luminescence of Phenyl-phenanthridine Dye on Aggregated Small Silver Nanoparticles", in J. Phys. Chem. B., **vol. 109**, 2005, pp. 8701–8706. https://doi.org/10.1021/jp046016j; (b) *N. Tka, M.A.H Ayed, M.B Braiek, M. Jabli, N. Chaaben, K. Alimi, S. Jopp, P. Langer*, "2,4-Bis(arylethynyl)-9-chloro-5,6,7,8-tetrahydroacridines: synthesis and photophysical properties", in Beilstein J Org Chem., **vol. 17**, 2021, pp. 1629-1640 https://doi: 10.3762/bjoc.17.115 ; (c) *N. Tka, M.A.H. Ayed, M.B. Braiek, M. Jabli, P. Langer*, Synthesis and investigation on optical and electrochemical properties of 2,4-diaryl-9-chloro-5,6,7,8-tetrahydroacridines, *Beilstein J. Org. Chem.* **2021,** *17*, 2450–2461. https://doi.org/10.3762/bjoc.17.162
[14]. *M.M. Hrubaru, F.A. Ngounoue Kamga, N. Murat, C. Draghici, M.-R. Bujduveanu, E.-M. Ungureanu, E. Diacu*, "Electrochemical investigation on 1,2,3,4-tetrahydroacridine-9-carboxamide in different organic solvents", in Sci. Bull. U.P.B., Series B, 2024, **vol 86** (1), 31 – 46.
[15]. *A.-A Vasile, E.-M. Ungureanu, G. Stanciu, M. Cristea, A. Stefaniu*, "Evaluation of (Z)-5-(Azulen-1-ylmethylene)-2-thioxothiazolidin-4-ones Properties Using Quantum Mechanical Calculations", in Symmetry, **vol. 13**, 2021, pp. 1462, https://doi.org/10.3390/sym13081462
[16]. *O. Ciocirlan, E.-M. Ungureanu, A.-A. Vasile, A. Stefaniu*, "Properties Assessment by Quantum Mechanical Calculations for Azulenes Substituted with Thiophen– or Furan–Vinyl–Pyridine", in Symmetry, **vol. 14**, 2022, pp. 354 https://doi.org/10.3390/sym14020354
[17]. (a) *M.M. Hrubaru, B. Drăghici, M. Plaveţi, M. Maganu, F.D. Badea*, "New tetrahydroacridine derivatives having as precursor the acid 1,2,3,4-tetrahydroacridin-9-carboxilic"- in Rev. Chim., **vol. 56**, 2005, pp. 301-304. (b) *M.M. Hrubaru, B. Draghici, A. Perescu, F. Badea*, "Synthesis and Spectral Characterisation of Some Substituted Benzamides Deriving from 7-Methoxy-9-Amino-1,2,3,4-Tetrahydroacridines", in Rev. Chim., **vol. 55**, 2004, pp. 773-776. (c) *B. Drăghici, M.M. Hrubaru, M. Plaveti, M. Maganu, E. Haţieganu*, "Synthesis and Spectral Characterization of some Tetrahydroacridin-9-Carbanilides", in Rev. Chim., **vol. 57**, 2006, pp. 951-954
[18]. *M. Carje*, "Űber 1,2,3 4-Tetrahydroakridin-9-Carboxyl-Säure-derivate", in Rev. Roum. Chem, **vol. 18**, no. 6, 1973, pp.1013-1016
[19]. *J. Bielawsky*, "Analogues of 9-amino-1,2,3,4-tetrahydroacridine", in Coll. Czech. Chim. Commun., **vol. 42**, 1977, pp.2802-2808, https://doi.org/10.1135/cccc19772802
[20]. (a) *M.M. Hrubaru. B. Draghici. A. Perescu. F. Badea*, "Synthesis and Spectral Characterization of Some Substituted Benzamides Deriving from 7-Methoxy-9-Amino-1.2.3.4-Tetrahydroacridines", in Rev. Chim., **vol. 55**, 2004. pp. 773-776.

[21]. *F.A. Ngounoue Kamga. M.-M. Hrubaru. O. Enache. E. Diacu. C. Draghici. V. Tecuceanu. E.-M. Ungureanu. S. Nkemone. P.T. Ndifon,* "Ni(II)-Salophen—Comprehensive Analysis on Electrochemical and Spectral Characterization and Biological Studies", in Molecules, **vol. 28**, 2023, pp. 5464, https://doi.org/10.3390/molecules28145464

[22]. a). *W.J. Hehre*, "A Guide to Molecular Mechanics and Quantum Chemical Calculations", Wavefunction, Inc.: Irvine, CA, USA, 2003. (b). *C. Lee, W. Yang, R.G. Parr*, "Development of the Colle-Salvetti correlation-energy formula into a functional of the electron density", in Phys. Rev. B, **vol. 37**, 1988, pp. 785–789

[23]. *Y. Shao, L.F. Molnar, Y. Jung, J. Kussmann, C. Ochsenfeld, S.T. Brown, A.T.B. Gilbert, L.V. Slipchenko, S.V. Levchenko, D.P. O'Neill,* et al. "Advances in methods and algorithms in a modern quantum chemistry program package", in Phys. Chem. Chem. Phys. **vol. 8**, 2006, pp. 3172–3191

[24]. *D.D. Méndez-Hernández, P. Tarakeshwar, D. Gust, T.A. Moore, A.L. Moore, V. Mujica,* "Simple and accurate correlation of experimental redox potentials and DFT-calculated HOMO/LUMO energies of polycyclic aromatic hydrocarbons", in J. Mol. Model. **vol. 19**, 2013, pp. 2845–2848

[25]. *A. Zarrouk, H. Zarrok, R. Salghi, B. Hammouti, S.S. Al-Dey ab, R. Touzani, M. Bouachrine, I. Warad, T.B. Hadda*, "A theoretical investigation on the corrosion inhibition of copper by quinoxaline derivatives in nitric acid solution", in Int. J. Electrochem. Sci., 2012, **vol. 7**, pp. 6353–6364

[26]. *H. Wang, X. Wang, H. Wang, L. Wang, A. Liu*, "DFT study of new bipyrazole derivatives and their potential activity as corrosion inhibitors", in J. Mol. Model., **vol. 13**, 2007, pp. 147–153

[27]. *R.G. Parr, L. Szentpaly, S. Liu*, "Electrophilicity Index", in J. Am. Chem. Soc., **vol. 121**, 1999, pp. 1922–1924

[28]. *V.S. Sastri, J.R. Perumareddi*, "Molecular orbital theoretical studies of some organic corrosion inhibitors", in Corros. Sci., **vol. 53**, 1997, pp. 617–622

[29]. R. *Yankova, S. Genieva, N. Halachev, G. Dimitrova*, "Molecular structure, vibrational spectra, MEP, HOMO-LUMO and NBO analysis of $Hf(SeO_3)(SeO_4)(H_2O)_4$", in J. Mol. Struct., **vol. 1106**, 2016, pp. 82–88

[30]. *R. G. Pearson, J. Songstad*, "Application of the Principle of Hard and Soft Acids and Bases to Organic Chemistry," in J. Am. Chem. Soc., **vol. 89**, 1967, pp. 1827–1836

[31]. *Pearson, R.G.* "Recent Advances in the Concept of Hard and Soft Acids and Bases", in J. Chem. Educ. 1987, **vol. 64**, pp. 561–567